Solving the 2-D Scalar Radiative Transfer Equation

Manuel Alejandro Jaimes Caballero & Roel Snieder
Center for Wave Phenomena and Dept. of Geophysics, Colorado School of Mines, Golden CO 80401
mjaimescaballero@mymail.mines.edu

ABSTRACT
We propose an energy-conserving time-stepping algorithm for solving the 2-D scalar radiative transfer equations with angle-dependent scattering. We derive the analytical solution to the radiative transfer equations for a given direction of propagation with an initial condition and an arbitrary scattering function. We discretize this solution for a number of propagation directions and take care of the advection of energy analytically. For a given direction of propagation the specific intensity at the current time depends on the specific intensities for other directions. This leads to a coupled system of equations where we solve for the specific intensities for all directions of propagation. To solve this coupled system of equations we construct an implicit time-stepping algorithm where we introduce weighting coefficients that allow us to conserve the energy in the numerical domain. We use the Henyey-Greenstein scattering function to specify the angle-dependent scattering, but other functions may be used, provided that they are normalized to conserve energy. We show numerical tests for isotropic and angle-dependent (forward) scattering. With our scheme we are able to conserve the energy in the numerical domain within 1% at times as large as ten scattering mean free times. The numerical intensities computed with our algorithm account for the spatio-temporal distribution of the wave energy transport and may be used to construct accurate sensitivity kernels, which are used in the theory of coda wave interferometry to quantify the spatial distribution of time-lapse medium changes.

Key words: Wave energy transport, angle-dependent scattering, numerical intensities, radiative transfer, coda wave interferometry

1 Introduction

Monitoring time-lapse changes in medium properties is of importance for a variety of applications in quantitative seismology. Some of these applications include, but are not limited to, volcano monitoring (Chouet, 1996), monitoring of land slides (Whiteley et al., 2019), time-lapse reservoir characterization (Vasco et al., 2015), monitoring of nuclear waste disposal sites (Nyberg et al., 2013), monitoring of geotechnical structures (Nakata and Snieder, 2014; Planès et al., 2016), nondestructive testing (Al Gharawi et al., 2019), and subsurface stress changes (Grêt et al., 2006).

To quantify the time-lapse seismic changes in medium properties one typically uses either singly scattered waves (e.g., primarily refracted waves used in standard seismic imaging (Claerbout, 1985)) or multiply scattered waves (Snieder, 2002; Snieder, 2006). Coda wave interferometry (CWI) has gained popularity as a method to quantify time-lapse seismic changes. This technique exploits the information contained in the multiply scattered waves which propagate through a medium. These waves spend more time in the propagation medium than the direct wave or single scattered waves, and therefore are more sensitive to perturbations in the medium properties as compared to the direct wave or singly scattered waves. The main idea behind CWI is to measure the seismic wave forms before and after a perturbation, and cross-correlate them to determine the imprint of the perturbation on the multiply scattered waves.

CWI has been used mostly to quantify either global (Grêt et al., 2006) or distributed velocity changes (Pacheco and Snieder, 2005) in an acoustic medium. More recently Snieder et al. (2019) extend CWI to elastic media. Rossetto et al. (2011) and Planès et al. (2014) extend CWI to study time-lapse structural changes via a decorrelation approach. Other types of perturbations such as the change in the location of scatterers (Snieder, 2002) or the relative location of seismic sources (Snieder and Vrijlandt, 2005) have also been investigated using CWI.

When the perturbation is distributed over space (either a spatially varying velocity or a change in scattering strength) one must compute a sensitivity kernel which describes how the wave energy interacts with the perturbations in the medium. In most CWI studies involving localized perturbations the sensitivity kernels, which depend on the wave intensity, are computed via one of the following approaches:

- Using the diffusion approximation which is only valid at times much larger than the transport mean free time (Rossetto et al., 2011; Planès et al., 2014; Snieder et al., 2019).
- Employing analytical solutions of the radiative transfer equation assuming a point-like, isotropic, impulsive source of intensity in a statistically homogeneous medium (Margerin et al., 2016).
- Solving the radiative transfer equation via the seismic particle method for an arbitrary medium (Przybilla et al., 2006; Zhang et al., 2021).
- Performing numerical simulations of the seismic wave field over several realizations of an arbitrarily heterogeneous acoustic or elastic medium (Kanu and Snieder, 2015; Snieder et al., 2019; Duran et al., 2020).

The diffusion approximation, as mentioned above, works well only for times much larger than the transport mean free time. Analytical solutions to the radiative transfer equations are inaccurate when either the source or medium properties are complicated. The seismic particle method, although quite accurate and applicable in complicated media, is computationally expensive and relies on using enough "seismic phonons" to sample the medium. Computation of the seismic wavefield over several realization of a medium has been widely used because it provides a connection between the wave equation and radiative transfer. However, there are two issues with this approach. First, the intensities must be averaged over enough realizations of the numerical medium to reduce statistical fluctuations. The second issue, which is arguably more significant than the first issue, is that one must decompose the calculated wave field into different propagation directions to properly account for the directionality of the wave energy transport.

In search of a method that overcomes some of the limitations mentioned above we propose a novel numerical scheme to compute the numerical intensities needed in the construction of the sensitivity kernels. Our approach is based on solving the scalar radiative transfer equation as an energy conserving time-stepping algorithm. Contrary to standard finite difference (FD) methods we handle the advection of energy analytically. This means that our numerical procedure for computing the wave energy transport does not introduce the usual numerical dispersion appearing in FD schemes due to the discretization of the difference operators. This numerical dispersion can produce negative solutions, which are unphysical because the intensities are nonnegative. Since the time discretization depends on the transport mean free time, instead of the frequency of the waves, the space and time discretization in the numerical modeling of the radiative transfer equation can be much coarser than it is for wave field modelling.

This paper is organized as follows: In section 2 we discuss the scalar equations of radiative transfer and derive a localized energy conserving time-stepping algorithm. In section 3 we show numerical simulations for both isotropic and an angle-dependent scattering media, and how energy is numerically conserved. In section 4 we discuss the relevance of our algorithm to calculate more accurate sensitivity kernels, and how our scheme may be extended to media where the velocity and scattering properties depend on space.

2 Numerical Solutions to the Scalar Radiative Transfer Equations

2.1 Description of the scalar equations of radiative transfer

The radiative transfer equation (RTE) is an integro-differential equation which describes the distribution of energy in a scattering medium as a function of space, time, and direction $\hat{\mathbf{n}}$ of wave propagation (Chandrasekhar, 1960). For late times, when the wave propagation is almost independent of direction, the equation of radiative transfer leads to diffusive wave transport (van Rossum and Nieuwenhuizen, 1999). The radiative transfer equation accurately describes wave transport at both early and late times, as well as the transition from ballistic wave propagation to weak scattering to strong multiple scattering (Paasschens, 1997). Despite its usefulness in describing energy transport, RTE is complicated and numerically demanding due to its dependence on not only space and time, but also on the directions of wave propagation. In 2 dimensions the radiative transfer solution depends on 4 variables (time, two space variables, and one angle). In 3 dimensions it depends on 6 variables (time, three space variables, and two angles).

The radiative transfer equation for scalar waves reads (Chandrasekhar, 1960; Özışık, 1973)

$$\frac{\partial I(\mathbf{r},\hat{\mathbf{n}},t)}{\partial t} + v(\mathbf{r})\hat{\mathbf{n}}\cdot\nabla I(\mathbf{r},\hat{\mathbf{n}},t) = -q(\mathbf{r})I(\mathbf{r},\hat{\mathbf{n}},t) + \oint S(\mathbf{r},\hat{\mathbf{n}},\hat{\mathbf{n}}')I(\mathbf{r},\hat{\mathbf{n}}',t)d^2\hat{\mathbf{n}}'. \tag{1}$$

In this expression the variable $I(\mathbf{r},\hat{\mathbf{n}},t)$ is the intensity of waves at a location $\mathbf{r}$ and time t propagating in the direction $\hat{\mathbf{n}}$. In the literature of radiative transfer the variable $I(\mathbf{r},\hat{\mathbf{n}},t)$ is referred to as the *specific intensity* (Chandrasekhar, 1960). The advection

of the energy, propagating with a wave velocity $v(\mathbf{r})$, is described by the term $v(\mathbf{r})\hat{\mathbf{n}} \cdot \nabla$. The term $q(\mathbf{r})I(\mathbf{r}, \hat{\mathbf{n}}, t)$ accounts for the energy that is lost to other directions in the propagation process. The term $\oint S(\mathbf{r}, \hat{\mathbf{n}}, \hat{\mathbf{n}}')I(\mathbf{r}, \hat{\mathbf{n}}', t)d^2\hat{\mathbf{n}}'$ describes the gain due to energy scattered from other directions.

2.2 Construction of the numerical algorithm

Using the notation from Wu (1985), and ignoring intrinsic attenuation, we write the radiative transfer equation as

$$\frac{\partial I(\mathbf{r}, \hat{\mathbf{n}}, t)}{\partial t} + v\hat{\mathbf{n}} \cdot \nabla I(\mathbf{r}, \hat{\mathbf{n}}, t) = -\frac{1}{\tau_s} I(\mathbf{r}, \hat{\mathbf{n}}, t) + \frac{1}{\tau_s} \oint f(\hat{\mathbf{n}}, \hat{\mathbf{n}}')I(\mathbf{r}, \hat{\mathbf{n}}', t)d^2\hat{\mathbf{n}}', \tag{2}$$

where for simplicity of notation we have dropped the spatial dependence on the velocity of wave propagation v and the scattering mean free time τ_s. The scattering mean free time corresponds to the average time between scattering events. The scattering function $f(\hat{\mathbf{n}}, \hat{\mathbf{n}}')$ relates the incident intensity to scattered intensity. In the continuous formulation this function is normalized such that

$$\oint f(\hat{\mathbf{n}}, \hat{\mathbf{n}}')d^2\hat{\mathbf{n}}' = 1. \tag{3}$$

This normalization follows by analyzing eqn. 2 for a homogeneous and time-independent intensity. Since we discretize the number of angular propagation directions we normalize the scattering function in the discrete sense

$$\sum_{\hat{\mathbf{n}}'} f(\hat{\mathbf{n}}, \hat{\mathbf{n}}') = 1, \tag{4}$$

where the discrete sum is implied to be over N discretization angles.

We proceed to write the radiative transfer equation in the following form

$$\frac{\partial I(\mathbf{r}, \hat{\mathbf{n}}, t)}{\partial t} + v\hat{\mathbf{n}} \cdot \nabla I(\mathbf{r}, \hat{\mathbf{n}}, t) = -\frac{1}{\tau_s} I(\mathbf{r}, \hat{\mathbf{n}}, t) + \frac{1}{\tau_s} \sum_{\hat{\mathbf{n}}'} f(\hat{\mathbf{n}}, \hat{\mathbf{n}}')I(\mathbf{r}, \hat{\mathbf{n}}', t). \tag{5}$$

For convenience we split the discrete sum on the right-hand side into $\sum_{\hat{\mathbf{n}}'=\hat{\mathbf{n}}}$ and $\sum_{\hat{\mathbf{n}}'\neq\hat{\mathbf{n}}}$

$$\frac{\partial I(\mathbf{r}, \hat{\mathbf{n}}, t)}{\partial t} + v\hat{\mathbf{n}} \cdot \nabla I(\mathbf{r}, \hat{\mathbf{n}}, t) = \left(-\frac{1}{\tau_s} + \frac{1}{\tau_s} f(\hat{\mathbf{n}}, \hat{\mathbf{n}}) \right) I(\mathbf{r}, \hat{\mathbf{n}}, t) + \frac{1}{\tau_s} \sum_{\hat{\mathbf{n}}'\neq\hat{\mathbf{n}}} f(\hat{\mathbf{n}}, \hat{\mathbf{n}}')I(\mathbf{r}, \hat{\mathbf{n}}', t). \tag{6}$$

In 2-dimensions, using $\hat{\mathbf{n}} = (\cos(\theta), \sin(\theta))$ and $\nabla = (\frac{\partial}{\partial x}, \frac{\partial}{\partial y})$, eqn. 6 becomes

$$\begin{aligned}\frac{\partial I(x, y, \hat{\mathbf{n}}, t)}{\partial t} + v\left(\cos(\theta)\frac{\partial I(x, y, \hat{\mathbf{n}}, t)}{\partial x} + \sin(\theta)\frac{\partial I(x, y, \hat{\mathbf{n}}, t)}{\partial y} \right) &= \left(-\frac{1}{\tau_s} + \frac{1}{\tau_s} f(\hat{\mathbf{n}}, \hat{\mathbf{n}}) \right) I(x, y, \hat{\mathbf{n}}, t) \\ &+ \frac{1}{\tau_s} \sum_{\hat{\mathbf{n}}'\neq\hat{\mathbf{n}}} f(\hat{\mathbf{n}}, \hat{\mathbf{n}}')I(x, y, \hat{\mathbf{n}}', t).\end{aligned} \tag{7}$$

Defining $q = (1 - f(\hat{\mathbf{n}}, \hat{\mathbf{n}}))/\tau_s$, one can show that the solution to eqn. 7 is

$$\begin{aligned}&I(x, y, \hat{\mathbf{n}}, t) = I_0(x - vt\cos(\theta), y - vt\sin(\theta), \hat{\mathbf{n}})e^{-qt} \\ &+ \frac{1}{\tau_s} \int_0^t \sum_{\hat{\mathbf{n}}'\neq\hat{\mathbf{n}}} f(\hat{\mathbf{n}}, \hat{\mathbf{n}}')I(x - v(t - t')\cos(\theta), y - v(t - t')\sin(\theta), \hat{\mathbf{n}}', t')e^{-q(t-t')}dt'.\end{aligned} \tag{8}$$

Note that the advection of the energy transport is taken care of by the arguments $x - vt\cos(\theta)$, $y - vt\sin(\theta)$, $x - v(t - t')\cos(\theta)$, and $y - v(t - t')\sin(\theta)$. By analytically handling the advection of the wave energy transport we avoid numerical dispersion in our solution and we are able to use a larger discretization step in space and time. Avoiding numerical dispersion is important when modeling intensities, since numerical dispersion might lead to negative intensities, which is unphysical.

To apply expression (8) as a time-marching algorithm we replace $0 \to t - \Delta t$

$$\begin{aligned}&I(x, y, \hat{\mathbf{n}}, t) = I(x - v\Delta t\cos(\theta), y - v\Delta t\sin(\theta), \hat{\mathbf{n}}, t - \Delta t)e^{-q\Delta t} \quad + \\ &\frac{1}{\tau_s} \int_{t-\Delta t}^t \sum_{\hat{\mathbf{n}}'\neq\hat{\mathbf{n}}} f(\hat{\mathbf{n}}, \hat{\mathbf{n}}')I(x - v(t - t')\cos(\theta), y - v(t - t')\sin(\theta), \hat{\mathbf{n}}', t')e^{-q(t-t')}dt'.\end{aligned} \tag{9}$$

We then write the time integral on the right-hand side in the form

$$\int_{t-\Delta t}^t h(t)dt = \Big[Ah(t - \Delta t) + Bh(t) \Big] \Delta t, \tag{10}$$

by which eqn. 9 becomes

$$I(x,y,\hat{\mathbf{n}},t) = I(x - v\Delta t\cos(\theta), y - v\Delta t\sin(\theta), \hat{\mathbf{n}}, t-\Delta t)e^{-q\Delta t}$$
$$+\frac{A}{\tau_s}\sum_{\hat{\mathbf{n}}'\neq\hat{\mathbf{n}}} f(\hat{\mathbf{n}},\hat{\mathbf{n}}')I(x - v\Delta t\cos(\theta), y - v\Delta t\sin(\theta), \hat{\mathbf{n}}', t-\Delta t)e^{-q\Delta t}\Delta t$$
$$+\frac{B}{\tau_s}\sum_{\hat{\mathbf{n}}'\neq\hat{\mathbf{n}}} f(\hat{\mathbf{n}},\hat{\mathbf{n}}')I(x,y,\hat{\mathbf{n}}',t)\Delta t. \tag{11}$$

We then rearrange eqn 11 to obtain

$$I(x,y,\hat{\mathbf{n}},t) - \frac{B}{\tau_s}\sum_{\hat{\mathbf{n}}'\neq\hat{\mathbf{n}}} f(\hat{\mathbf{n}},\hat{\mathbf{n}}')I(x,y,\hat{\mathbf{n}}',t)\Delta t$$
$$= I(x - v\Delta t\cos(\theta), y - v\Delta t\sin(\theta), \hat{\mathbf{n}}, t-\Delta t)e^{-q\Delta t}$$
$$+\frac{A}{\tau_s}\sum_{\hat{\mathbf{n}}'\neq\hat{\mathbf{n}}} f(\hat{\mathbf{n}},\hat{\mathbf{n}}')I(x - v\Delta t\cos(\theta), y - v\Delta t\sin(\theta), \hat{\mathbf{n}}', t-\Delta t)e^{-q\Delta t}\Delta t. \tag{12}$$

This results in a system of N equations, with N variables (the intensities at every discretization angle). For an arbitrary number of N directions we write

$$\begin{bmatrix} 1 & \cdots & -\frac{B\Delta t}{\tau_s} f(\hat{\mathbf{n}}_i,\hat{\mathbf{n}}_j) \\ & & \\ -\frac{B\Delta t}{\tau_s} f(\hat{\mathbf{n}}_j,\hat{\mathbf{n}}_i) & \cdots & 1 \end{bmatrix} \begin{bmatrix} I(x,y,\hat{\mathbf{n}}_1,t) \\ I(x,y,\hat{\mathbf{n}}_2,t) \\ \\ I(x,y,\hat{\mathbf{n}}_N,t) \end{bmatrix} = \begin{bmatrix} S(x,y,\hat{\mathbf{n}}_1,t-\Delta t) \\ S(x,y,\hat{\mathbf{n}}_2,t-\Delta t) \\ \\ S(x,y,\hat{\mathbf{n}}_N,t-\Delta t) \end{bmatrix}. \tag{13}$$

The entries of the vector on the right-hand side of eqn. 13 correspond to the right-hand side of eqn. 12. For a given direction $\hat{\mathbf{n}}_i$

$$S(x,y,\hat{\mathbf{n}}_i,t-\Delta t) = I(x - v\Delta t\cos(\theta), y - v\Delta t\sin(\theta), \hat{\mathbf{n}}_i, t-\Delta t)e^{-q\Delta t}$$
$$+\frac{A}{\tau_s}\sum_{\hat{\mathbf{n}}'\neq\hat{\mathbf{n}}_i} f(\hat{\mathbf{n}},\hat{\mathbf{n}}')I(x - v\Delta t\cos(\theta), y - v\Delta t\sin(\theta), \hat{\mathbf{n}}', t-\Delta t)e^{-q\Delta t}\Delta t. \tag{14}$$

The $N \times N$ matrix on the left-hand side of eqn. 13 contains 1 on the diagonal and $-\frac{B\Delta t}{\tau_s} f(\hat{\mathbf{n}}_i,\hat{\mathbf{n}}_j)$ off-diagonal. The i and j indices correspond to the row and column of this matrix, respectively. The indices were introduced to emphasize that the scattering function $f(\hat{\mathbf{n}}_i,\hat{\mathbf{n}}_j)$ depends on the incident and scattering angles. This matrix multiplies the intensity vector that we solve for. The right hand-side corresponds to a source term with which we evolve the numerical solution, and depends on the intensities at the previous time, given by eqn. 14.

To evolve the specific intensities over time we numerically solve the system of equations 13. Notice, however, that we have yet to define the weighting coefficients A and B that were introduced in eqn. 10. We define these coefficients by the requirement that the total energy is conserved for the case of isotropic scattering. As we show in the appendix, this leads to

$$B = \frac{1 - \left(1 + \Delta t\frac{N-1}{N\tau_s}\right)e^{-q\Delta t}}{\Delta t\frac{N-1}{N\tau_s}\left(1 - e^{-q\Delta t}\right)}, \quad A = 1 - B, \tag{15}$$

with $q = (N-1)/N\tau_s$. For the case of angle-dependent scattering the formulation becomes much more complicated but we assume, for the time being, that the weighting coefficients remain the same.

2.3 Choice of scattering function

We use the Henyey-Greenstein (HG) function in 2D to describe a medium with arbitrary angle-dependent scattering. We use a discretized version of the HG function (Margerin et al., 2016)

$$f(\hat{\mathbf{n}},\hat{\mathbf{n}}') = \frac{1}{N}\frac{1-g^2}{(1+g^2-2g(\hat{\mathbf{n}}\cdot\hat{\mathbf{n}}'))}. \tag{16}$$

The variable g describes the level of angle-dependent scattering and it ranges from predominantly backward scattering ($g=-1$) to isotropic scattering ($g=0$) to predominantly forward scattering ($g=1$). N is the number of discretized angular directions.

We normalize the scattering function using eqn 4

$$\sum_{\hat{\mathbf{n}}'}\frac{1}{N}\frac{1-g^2}{(1+g^2-2g(\hat{\mathbf{n}}\cdot\hat{\mathbf{n}}'))} = 1, \tag{17}$$

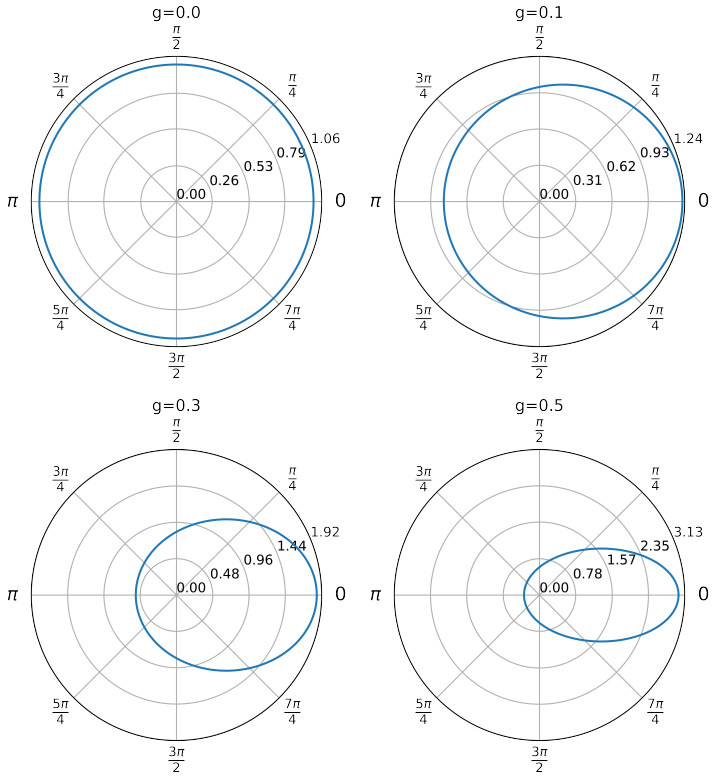

Figure 1. Radiation pattern of the Henyey-Greenstein scattering function for different values of g. The incident direction is aligned along the positive horizontal axis.

where the discrete sum is over N angles. To fulfill this requirement one needs a normalization constant in the left-hand side (except when the scattering is isotropic)

In the isotropic case the function is normalized for any number of N angles. To see this set $g = 0$ so that

$$\sum_{\hat{\mathbf{n}}'} \frac{1}{N} \frac{1-g^2}{(1+g^2-2g(\hat{\mathbf{n}}\cdot\hat{\mathbf{n}}'))} = \sum_{\hat{\mathbf{n}}'} \frac{1}{N} = \frac{1}{N} N = 1. \tag{18}$$

When scattering is angle-dependent ($g \neq 0$) the discrete sum does not equal unity. For this case the discretized scattering function reads

$$f(\hat{\mathbf{n}}, \hat{\mathbf{n}}') = \frac{1}{C} \frac{1}{N} \frac{1-g^2}{(1+g^2-2g(\hat{\mathbf{n}}\cdot\hat{\mathbf{n}}'))}, \tag{19}$$

with

$$C = \sum_{\hat{\mathbf{n}}'} \frac{1}{N} \frac{1-g^2}{(1+g^2-2g(\hat{\mathbf{n}}\cdot\hat{\mathbf{n}}'))}. \tag{20}$$

In addition to normalizing the scattering function when there is angle-dependent scattering, we need to consider how many angles suffice to sample the angle-dependent wave energy transport. Fig. 1 shows the radiation pattern of the Henyey-Greenstein scattering function for different values of the parameter g, when the incident propagation direction is along the positive horizontal axis. For other incident propagation directions we can rotate the radiation pattern. When the medium is isotropic a small number of angles suffices to accurately sample the wave energy transport because the intensities vary smoothly with direction. As forward scattering increases, the energy concentrates in the forward direction. If we use a small number of discretization angles we can not accurately capture the angle-dependent scattering, and the numerical algorithm will not converge to the solutions of the scalar radiative transfer equations.

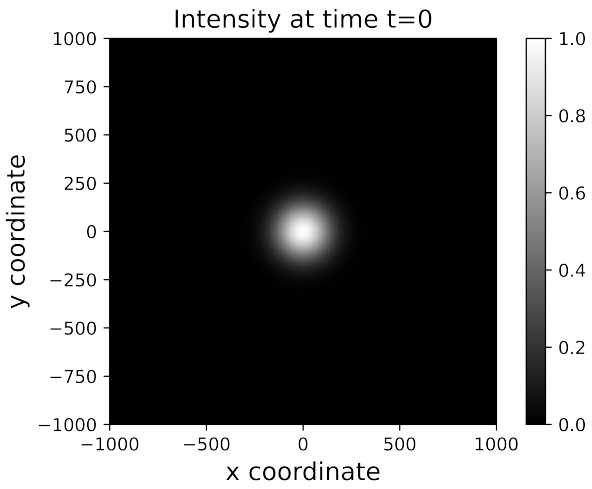

Figure 2. Total intensity at time $t = 0$. This intensity corresponds to the sum of the specific intensities over angular directions.

3 Numerical simulations

3.1 Choice of geometry and parameters

We consider a two dimensional medium with an intensity source placed at the middle of the domain, and set the specific intensities to be a fraction $1/N$ of the total intensity. The initial condition corresponds to a normalized Gaussian with a full width at half maximum ≈ 235 m , see Fig. 2. Both spatial coordinates range from -1000 m to 1000 m, with a grid spacing $\Delta x = \Delta y = 10$ m. We use a constant propagation velocity $v = 100$ m/s and scattering mean free time $\tau_s = 1$ s. We evolve the intensities from $t = 0$ to 10 s with $\Delta t = 0.1$ s, with the choice of temporal spacing small enough ($\Delta t \ll \tau_s$) to capture the scattering interactions, but not too small that the algorithm becomes computationally expensive. We use 16 directions of propagation, equally spaced, ranging from 0 to $15\pi/8$, and calculate the sum of the specific intensities at $t = 0, 1, 5, 10$ s to compute the total intensity. For this choice of parameters $v\Delta t/\Delta x = v\Delta t/\Delta y = 1$.

Notice that in eqn. 12 for some arbitrary choice of θ we evaluate the specific intensities at spatial locations which do not lie on a grid point. To remedy this we interpolate (via cubic splines) the specific intensities at the previous time step and use the interpolated values to evolve the specific intensities at the current time step.

3.2 Isotropic scattering

In the case of isotropic (or weakly angle-dependent) scattering a few angular directions are enough to describe the energy transport. This is because scattering has no preferred direction of propagation. Fig. 3 shows that the intensity spreads in the numerical domain over time and it does so diffusively. The intensity is nearly circular, even though we used only 16 directions of propagation for the specific intensities.

3.3 Angle-dependent scattering

Now we consider the case when we deal with angle-dependent scattering, using $g = 0.1, 0.3, 0.5$, respectively. For this case a more relevant parameter which quantifies the wave energy transport is the transport mean free time, τ^*. This quantity is related to the scattering mean free time by $\tau^* \approx \tau_s/(1-g)$ (Margerin et al., 2016). For the used values of g the corresponding transport mean free times are $\tau^* = 1.11, 1.43, 2.0$ s, respectively. Fig. 4 shows cross-sections of the intensity for several values of the parameter g, at different times t. The upper left panel shows the initial condition used in solving the radiative transfer equations. At an early time of $t = 1$ s (upper right panel) the difference in the intensities is small, and the angle-dependent scattering does not have a significant effect on the intensity. At a time $t = 5$ s (lower left panel) the effect of angle-dependent scattering is visible. As the value of g increases the intensity at $x = 0$ (peak of initial condition) decreases in value and the intensity at locations far from the origin increase in value. At large times (lower right panel) the intensities are significantly affected by angle-dependent scattering. Due to forward scattering the energy spreads out more quickly as g increases, and forward scattering becomes important in the energy transport. Fig. 5 shows the temporal evolution of the spatial width of the intensity for different levels of angle-dependent scattering. At early times the width of the intensity profile increases more rapidly with time as the value of g increases. At late times ($t \gg \tau_s$) the width of the intensity profile grows as $t^{1/2}$, which corresponds to diffusive transport.

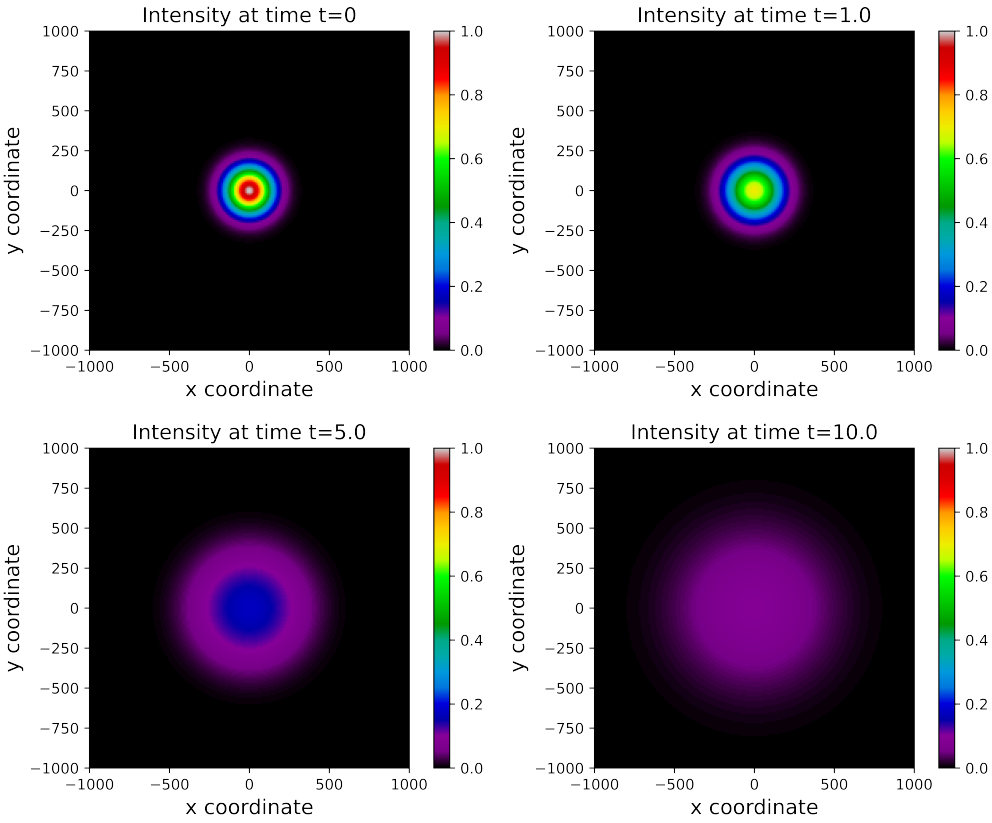

Figure 3. Total intensities at times $t = 0, 1, 5, 10$ s.

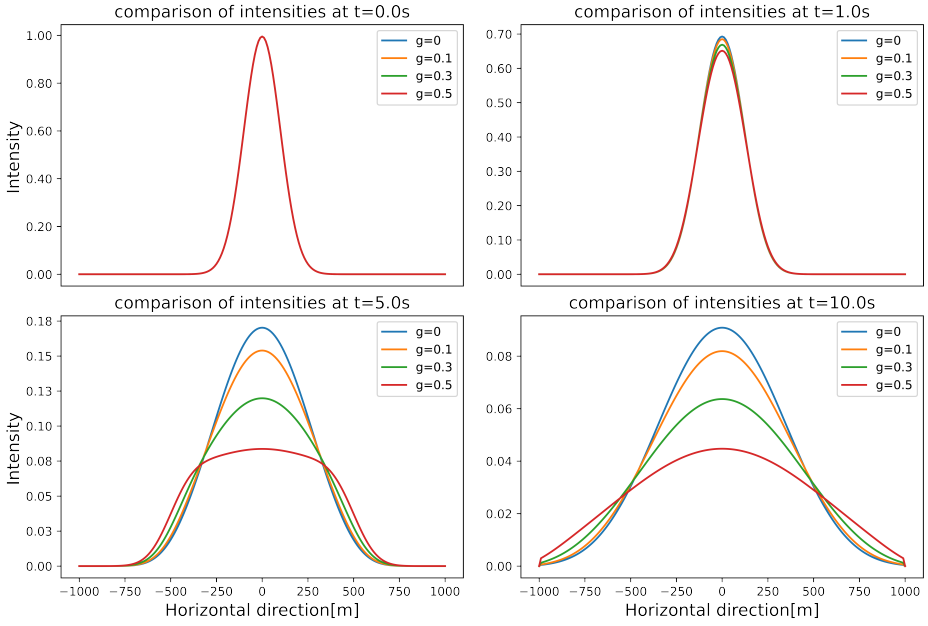

Figure 4. Cross-sections of the total intensity at $y = 0$ for different values of g at times $t = 0, 1, 5, 10$ s.

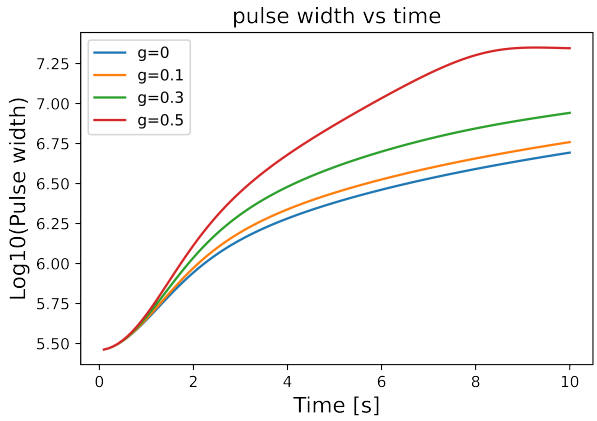

Figure 5. Width of the intensity profiles in Fig. 4 as a function of time for several values of g. The width is estimated using a Gaussian fit of the total intensity.

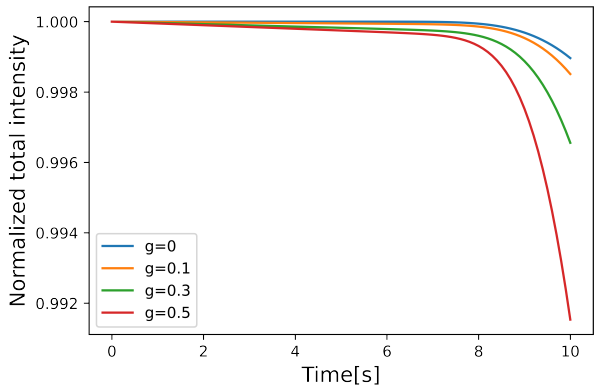

Figure 6. Normalized total intensity as a function of time for different values of the parameter g, and N =16. The total intensity at time t is normalized by the total initial intensity.

3.4 Numerical conservation of energy

To verify the accuracy of our algorithm we consider the total energy in the numerical domain. The total numerical energy must be conserved, as required by radiative transfer, until the time at which the energy reaches the edges of the computational domain. Fig. 6 shows that for $N = 16$, as the value of g increases the conservation of energy slightly degrades, less than 1%. This loss in total energy is for practical purposes not significant. The drop in the normalized total intensity near $t = 8$ s is due to the waves hitting the boundary, where we force the intensity to be equal to zero. At early times there is a tiny degradation in the conservation of energy as the value of g increases. There are two potential reasons for this behavior. The first reason is that we need more discretization angles to accurately sample the angle-dependent scattering in the wave energy transport. The second reason is that when the angle-dependent scattering increases the optimal weighting coefficients A and B might slightly change in value. At later times the degradation becomes more evident and the drop in the total energy occurs earlier with increasing angle-dependent scattering. This is because when forward scattering becomes significant, the wave energy reaches the boundary faster.

4 Discussion

The numerical algorithm that we propose to solve the scalar radiative transfer equations is derived from eqn. 2. It accurately accounts for the spatio-temporal distribution of the intensity and can be used to compute the specific intensities needed in the construction of the sensitivity kernels used in CWI. In our algorithm the specific intensities at the current time depend only on the specific intensities at the previous time step, a time-stepping approach. Our algorithm can incorporate any source distribution. For our choice of boundary conditions the conservation of energy does not hold once the wave energy reaches the boundaries. The proposed method can be used to compute the intensities in a medium with arbitrary angle-dependent scattering. The Henyey-

Greenstein scattering function was used to quantify scattering strength as a function of scattering angle. When the scattering strength changes significantly with scattering angle we must discretize the angular dependence of the specific intensity sufficiently fine to sample the radiation pattern of the scatterers. The numerical scheme, although derived for homogeneous media, can be extended to media whose scattering properties depend on position. In the numerical examples, our algorithm conserves the total energy in the medium to within 1% for times as large as ten scattering mean free times.

5 Conclusions

We proposed an energy-conserving time-stepping algorithm to solve the scalar radiative transfer equations. This algorithm accurately simulates wave transport for angle-dependent scattering. Our algorithm can be extended to media where the scattering properties depend on position. In our scheme we solve for the specific intensities required in the construction of the sensitivity kernels that are used in localized imaging via coda wave interferometry. By directly solving the scalar radiative transfer equations we obtain specific intensities which give accurate sensitivity kernels, and therefore provide an accurate description of the spatially-distributed perturbations, which is important to characterize and image time-lapse changes. Further work is required to extend our algorithm to 2D elastic media, 3-D acoustic and elastic media, and media where the velocity is not constant. When the medium is elastic we need to keep track of the modes of wave propagation and any conversions between modes that occur in the wave transport, which makes the radiative transfer equations more complicated.

Acknowledgements

This work is supported by the Consortium Project on Seismic Inverse Methods for Complex Structures at the Colorado School of Mines.

REFERENCES

Al Gharawi, M., Y. Adu-Gyamfi, and G. Washer, 2019, A framework for automated time-lapse thermography data processing: Construction and Building Materials, **227**, 116507.

Chandrasekhar, S., 1960, Radiative transfer: Dover Publications, New York.

Chouet, B. A., 1996, New Methods and Future Trends in Seismological Volcano Monitoring, *in* Monitoring and Mitigation of Volcano Hazards: Springer Berlin Heidelberg, 23–97.

Claerbout, J. F., 1985, Imaging the earth's interior: Blackwell Scientific Publications, Boston.

Duran, A., T. Planès, and A. Obermann, 2020, Coda-wave decorrelation sensitivity kernels in 2-D elastic media: a numerical approach: Geophysical Journal International, **223**, 934–943.

Grêt, A., R. Snieder, and U. Özbay, 2006, Monitoring in-situ stress changes in a mining environment with coda wave interferometry: Geophys. J. Int., **167**, 504–508.

Grêt, A., R. Snieder, and J. Scales, 2006, Time-lapse monitoring of rock properties with coda wave interferometry: Time-Lapse Monitioring of Rock Properties: Journal of Geophysical Research: Solid Earth, **111**, B03305.

Kanu, C., and R. Snieder, 2015, Numerical computation of the sensitivity kernel for monitoring weak changes with multiply scattered acoustic waves: Geophysical Journal International, **203**, 1923–1936.

Margerin, L., T. Planès, J. Mayor, and M. Calvet, 2016, Sensitivity kernels for coda-wave interferometry and scattering tomography: theory and numerical evaluation in two-dimensional anisotropically scattering media: Geophysical Journal International, **204**, 650–666.

Meyer, C. D., 2000, Matrix analysis and applied linear algebra: Society for Industrial and Applied Mathematics.

Nakata, N., and R. Snieder, 2014, Monitoring a Building Using Deconvolution Interferometry. II: Ambient-Vibration Analysis: Bulletin of the Seismological Society of America, **104**, 204–213.

Nyberg, S., U. Kallio, and H. Koivula, 2013, GPS monitoring of bedrock stability at Olkiluoto nuclear waste disposal site in Finland from 1996 to 2012: Journal of Geodetic Science, **3**, 121–126.

Paasschens, J. C. J., 1997, Solution of the time-dependent Boltzmann equation: Physical Review E, **56**, 1135–1141.

Pacheco, C., and R. Snieder, 2005, Time-lapse travel time change of multiply scattered acoustic waves: The Journal of the Acoustical Society of America, **118**, 1300–1310.

Planès, T., M. Mooney, J. Rittgers, M. Parekh, M. Behm, and s. t. Snieder, R., 2016, Time-lapse monitoring of internal erosion in earthen dams and levees using ambient seismic noise: Géotechnique, **66**, 301–312.

Planès, T., E. Larose, L. Margerin, V. Rossetto, and C. Sens-Schönfelder, 2014, Decorrelation and phase-shift of coda waves induced by local changes: multiple scattering approach and numerical validation: Waves in Random and Complex Media, **24**, 99–125.

Przybilla, J., M. Korn, and U. Wegler, 2006, Radiative transfer of elastic waves versus finite difference simulations in two-dimensional random media: Journal of Geophysical Research, **111**, B04305.

Rossetto, V., L. Margerin, T. Planès, and Larose, 2011, Locating a weak change using diffuse waves: Theoretical approach and inversion procedure: Journal of Applied Physics, **109**, 034903.

Snieder, 2006, The Theory of Coda Wave Interferometry: Pure and Applied Geophysics, **163**, 455–473.

Snieder, R., 2002, Coda Wave Interferometry for Estimating Nonlinear Behavior in Seismic Velocity: Science, **295**, 2253–2255.

Snieder, R., A. Duran, and A. Obermann, 2019, Locating velocity changes in elastic media with coda wave interferometry, *in* Seismic ambient noise: Cambridge University Press, 6, 188–217.

Snieder, R., and M. Vrijlandt, 2005, Constraining the source separation with coda wave interferometry: Theory and application to earthquake doublets in the Hayward fault, California: Source separations from seismic coda: Journal of Geophysical Research: Solid Earth, **110**.

van Rossum, M. C. W., and T. M. Nieuwenhuizen, 1999, Multiple scattering of classical waves: microscopy, mesoscopy, and diffusion: Reviews of Modern Physics, **71**, 313–371.

Vasco, D. W., A. Bakulin, H. Baek, and L. R. Johnson, 2015, Reservoir characterization based upon the onset of time-lapse amplitude changes: GEOPHYSICS, **80**, M1–M14.

Whiteley, J. S., J. E. Chambers, S. Uhlemann, P. B. Wilkinson, and J. M. Kendall, 2019, Geophysical Monitoring of Moisture-Induced Landslides: A Review: Reviews of Geophysics, **57**, 106–145.

Wu, R.-S., 1985, Multiple scattering and energy transfer of seismic waves – separation of scattering effect from intrinsic attenuation – I. Theoretical modelling: Geophysical Journal International, **82**, 57–80.

Zhang, T., C. Sens-Schönfelder, and L. Margerin, 2021, Sensitivity kernels for static and dynamic tomography of scattering and absorbing media with elastic waves: a probabilistic approach: Geophysical Journal International, **225**, 1824–1853.

Özışık, M. N., 1973, Radiative transfer and interactions with conduction and convection: Wiley.

Appendix

We rewrite eqn. 13 as

$$\begin{bmatrix} I(x,y,\hat{\mathbf{n}}_1,t) \\ I(x,y,\hat{\mathbf{n}}_2,t) \\ \\ I(x,y,\hat{\mathbf{n}}_N,t) \end{bmatrix} = \begin{bmatrix} 1 & \cdots & -\frac{B\Delta t}{\tau_s} f(\hat{\mathbf{n}}_i,\hat{\mathbf{n}}_j) \\ & \ddots & \\ -\frac{B\Delta t}{\tau_s} f(\hat{\mathbf{n}}_j,\hat{\mathbf{n}}_i) & \cdots & 1 \end{bmatrix}^{-1} \begin{bmatrix} S(x,y,\hat{\mathbf{n}}_1,t-\Delta t) \\ S(x,y,\hat{\mathbf{n}}_2,t-\Delta t) \\ \\ S(x,y,\hat{\mathbf{n}}_N,t-\Delta t) \end{bmatrix}, \tag{A-1}$$

and assume isotropic scattering so that $f(\hat{\mathbf{n}}_i,\hat{\mathbf{n}}_j) = 1/N$. The system of equations then reads

$$\begin{bmatrix} I(x,y,\hat{\mathbf{n}}_1,t) \\ I(x,y,\hat{\mathbf{n}}_2,t) \\ \\ I(x,y,\hat{\mathbf{n}}_N,t) \end{bmatrix} = \begin{bmatrix} 1 & \cdots & -\frac{B\Delta t}{N\tau_s} \\ & \ddots & \\ -\frac{B\Delta t}{N\tau_s} & \cdots & 1 \end{bmatrix}^{-1} \begin{bmatrix} S(x,y,\hat{\mathbf{n}}_1,t-\Delta t) \\ S(x,y,\hat{\mathbf{n}}_2,t-\Delta t) \\ \\ S(x,y,\hat{\mathbf{n}}_N,t-\Delta t) \end{bmatrix}, \tag{A-2}$$

where we can compute the inverse on the right-hand side analytically using the Sherman-Morrison formula and rank-1 updates (Meyer, 2000). We write the intensity vector solution as

$$\begin{bmatrix} I(x,y,\hat{\mathbf{n}}_1,t) \\ I(x,y,\hat{\mathbf{n}}_2,t) \\ \\ I(x,y,\hat{\mathbf{n}}_N,t) \end{bmatrix} = \xi \begin{bmatrix} (N-2)\frac{B\Delta t}{N\tau_s} - 1 & \cdots & -\frac{B\Delta t}{N\tau_s} \\ & \ddots & \\ -\frac{B\Delta t}{N\tau_s} & \cdots & (N-2)\frac{B\Delta t}{N\tau_s} - 1 \end{bmatrix} \begin{bmatrix} S(x,y,\hat{\mathbf{n}}_1,t-\Delta t) \\ S(x,y,\hat{\mathbf{n}}_2,t-\Delta t) \\ \\ S(x,y,\hat{\mathbf{n}}_N,t-\Delta t) \end{bmatrix},$$

$$\xi = \frac{1}{(N-1)\left(\frac{B\Delta t}{N\tau_s}\right)^2 + (N-2)\left(\frac{B\Delta t}{N\tau_s}\right) - 1}. \tag{A-3}$$

In compact form we write

$$\vec{I} = \boldsymbol{P}\vec{S} \tag{A-4}$$

The accuracy of this marching scheme depends on how we choose the parameters A and B that were introduced via eqn. 10. Since the equation of radiative transfer is based on conservation of energy, we choose A and B such that the total intensity in the domain is conserved between two consecutive times. That is, we want to choose A and B such that

$$E(t) = E(t-\Delta t), \tag{A-5}$$

where $E(t)$ is the sum over all discretization angles and all grid points of the numerical specific intensity. To this end we write eqn. A-4 in terms of the j direction

$$I(x,y,\hat{\mathbf{n}}_j,t) = \sum_{i=1}^{N} P_{ji} S(x,y,\hat{\mathbf{n}}_i, t-\Delta t), \tag{A-6}$$

where P_{ji} corresponds to the (j,i) entry of the matrix $\boldsymbol{P}$. Summing over the angular directions we have

$$\sum_{j=1}^{N} I(x,y,\hat{\mathbf{n}}_j,t) = \sum_{j=1}^{N}\sum_{i=1}^{N} P_{ji} S(x,y,\hat{\mathbf{n}}_i, t-\Delta t). \tag{A-7}$$

Exchanging the summations on the right-hand side we get

$$\sum_{j=1}^{N} I(x,y,\hat{\mathbf{n}}_j,t) = \sum_{i=1}^{N}\sum_{j=1}^{N} P_{ji} S(x,y,\hat{\mathbf{n}}_i, t-\Delta t) = \sum_{i=1}^{N}\left(S(x,y,\hat{\mathbf{n}}_i, t-\Delta t)\sum_{j=1}^{N} P_{ji}\right). \tag{A-8}$$

Noting that $\sum_{j=1}^{N} P_{ji}$ is independent of i we write

$$\sum_{j=1}^{N} I(x,y,\hat{\mathbf{n}}_j,t) = \sum_{j=1}^{N} P_{ji} \sum_{i=1}^{N} S(x,y,\hat{\mathbf{n}}_i, t-\Delta t). \tag{A-9}$$

The left-hand side of this equation corresponds to the sum of the specific intensity over all angles, $I(x,y,t)$. Using eqn. 14 (with $g=0$) we obtain

$$\begin{aligned} I(x,y,t) = \sum_{j=1}^{N} P_{ji}\Bigg(&\sum_{i=1}^{N} I(x - v\Delta t\cos(\theta_i), y - v\Delta t\sin(\theta_i), \hat{\mathbf{n}}_i, t-\Delta t) e^{-q\Delta t} \\ &+ \frac{A}{N\tau_s}\sum_{i=1}^{N}\sum_{\hat{\mathbf{n}}'\neq\hat{\mathbf{n}}} I(x - v\Delta t\cos(\theta_i), y - v\Delta t\sin(\theta_i), \hat{\mathbf{n}}', t-\Delta t) e^{-q\Delta t}\Delta t\Bigg), \end{aligned} \tag{A-10}$$

with $q = (N-1)/N\tau_s$.

Taylor expanding the intensities on the right-hand side to first order in Δt around $(x,y,t-\Delta t)$ gives

$$\begin{aligned} I(x,y,t) = \sum_{j=1}^{N} P_{ji}\Bigg(&I(x,y,t-\Delta t) - \sum_{i=1}^{N} v\Delta t\cos(\theta_i)\partial_x I(x,y,\hat{\mathbf{n}}_i,t-\Delta t) \\ &- \sum_{i=1}^{N} v\Delta t\sin(\theta_i)\partial_y I(x,y,\hat{\mathbf{n}}_i,t-\Delta t) + \frac{A(N-1)\Delta t}{N\tau_s} I(x,y,t-\Delta t) \\ &- \frac{A\Delta t}{N\tau_s}\sum_{i=1}^{N} v\Delta t\cos(\theta_i)\partial_x I(x,y,t-\Delta t) \\ &- \frac{A\Delta t}{N\tau_s}\sum_{i=1}^{N} v\Delta t\sin(\theta_i)\partial_y I(x,y,t-\Delta t) \\ &+ \frac{A\Delta t}{N\tau_s}\sum_{i=1}^{N} v\Delta t\cos(\theta_i)\partial_x I(x,y,\hat{\mathbf{n}}_i,t-\Delta t) \\ &+ \frac{A\Delta t}{N\tau_s}\sum_{i=1}^{N} v\Delta t\sin(\theta_i)\partial_y I(x,y,\hat{\mathbf{n}}_i,t-\Delta t)\Bigg) e^{-q\Delta t}. \end{aligned} \tag{A-11}$$

We integrate over space and set the energy fluxes at the boundary equal to zero so that the terms involving spatial partial derivatives vanish. This gives

$$E(t) = \left(\sum_{j=1}^{N} P_{ji}\right) e^{-q\Delta t}\left(1 + \frac{(N-1)A\Delta t}{N\tau_s}\right) E(t-\Delta t). \tag{A-12}$$

Using

$$\sum_{j=1}^{N} P_{ji} = \frac{-\left(\frac{B\Delta t}{N\tau_s}\right) - 1}{(N-1)\left(\frac{B\Delta t}{N\tau_s}\right)^2 + (N-2)\left(\frac{B\Delta t}{N\tau_s}\right) - 1}, \tag{A-13}$$

and constraining the weights A and B to be normalized such that $A + B = 1$, we obtain expression 15.